The Prediction of Dynamic Fracture Evolution in PMMA using a Cohesive Zone Model

N. Murphy* and A. Ivankovic

Department of Mechanical Engineering, University College Dublin, Ireland
*Corresponding author. Email address: Neal.Murphy@ucd.ie

Abstract

A cohesive zone model was used in conjunction with the finite volume method to model the dynamic fracture of single edge notched tensile specimens of PMMA under essentially static loading conditions. In this study, the influence of the shape of the cohesive law was investigated, whilst keeping the cohesive strength and separation energy constant. Cohesive cells were adaptively inserted between adjacent continuum cells when the normal traction across that face exceeded the cohesive strength of the material. The cohesive constitutive law was therefore initially rigid, and the effective elasticity of the material was unaltered prior to insertion of the cohesive cells. Notch depths ranging from 2.0 mm to 0.1 mm were considered. The numerical predictions were compared with experimental observations for each notch depth and excellent qualitative and quantitative agreement was achieved in most cases. Following an initial period of rapid crack tip acceleration up to terminal velocities well below the Rayleigh wave speed, subsequent propagation took place at a constant rate under conditions of increasing energy flux to an expanding process region. In addition, attempted and successful branching was predicted for the shorter notches. It was found that the shape of the cohesive law had a significant influence on the dynamic fracture behaviour. In particular, the value of the initial slope of the softening function was found to be an important parameter. As the slope became steeper, the predicted terminal crack speed increased and the extent of the damage decreased.

1. Introduction

The continuum theory of linear elastodynamic fracture mechanics [1,2] fails to explain certain experimental observations that have been made for a wide range of brittle materials, particularly at higher crack speeds. Rather than accelerating to the Rayleigh wave speed, cracks tend to propagate at much lower mean velocities under conditions of increasing energy flux into the tip region. This is accompanied by an expansion of the fracture process region and an increase in fracture surface roughness and subsurface damage. In addition, attempted and successful crack branching is often observed.

The failure of classical elastodynamic fracture theory to explain these experimental observations lies primarily in the assumption that the dimensions of the fracture process region are considered to be negligible in comparison to the crack length and that the crack tip simply acts as an energy sink during crack propagation. Broberg [2] refers to this as the point model. As noted by Ravi-Chandar [3], this model ignores the fact that the fracture process zone can become quite large and that the dynamics of its evolution, regardless of the details of the separation processes in this region, can be quite independent of the wave propagation in the surrounding elastic body.

In the following pages, the merits and pitfalls of cohesive zone models will be discussed in this context. A series of experimental test results will be presented, characterizing the dynamic fracture behaviour of small tensile PMMA specimens. These tests will then be modelled using several different cohesive characteristics to describe the material behaviour in the fracture process region, and the results of these simulations will be compared with the experimental observations.

2. The cohesive zone model

2.1. The case for cohesive models

A cohesive view of materials addresses the shortcomings of classical continuum fracture mechanics by incorporating a cohesive strength and specific fracture energy into the material description. In principle, these parameters should be obtainable experimentally and this, combined with the ease with which cohesive models can be incorporated into standard analysis software, has led to their extensive use in computational fracture simulations. However, as noted in a recent review by Klein et al. [4], the fracture processes in a given material may be numerous and complicated. The size of the process zone ranges from near the angstrom length scale in ideally brittle crystals to the micron scale in polymers. The inherently small scale of the fracture processes implies that considerable computational effort is required for even modest specimen sizes.

Two aspects of cohesive zone modelling deserve particular attention. The first is whether the cohesive constitutive relation is taken to be initially elastic or initially rigid. The second concerns the assumed shape of this constitutive relation and its experimental or theoretical determination.

2.2. Initially elastic and initially rigid cohesive laws

In the first case, as the cohesive surfaces ‘separate’, the magnitude of the cohesive traction at first increases, reaches a maximum and then decreases to zero with increasing separation. The cohesive law therefore exhibits an elastic initial response due to the finite initial slope of the traction-separation curve, as shown in Fig. 1(a). This type of traction-separation law has been used extensively since its introduction in this context by Xu and Needleman [5] to model dynamic fracture in brittle solids. When using this type of law, insertion of the cohesive surfaces into a model alters the effective elasticity of the material. Whilst this may be of little consequence if only a single layer of cohesive elements is used, the effect can be significant if the cohesive cells are inserted between many continuum cells in a finite element model, as in [5], or in a finite volume model, as in [6]. When using this type of cohesive law to study the dynamics of the fracture process region, a conflicting situation arises, as noted in [4] and [7]. As noted above, the length of the cohesive zone ahead of a crack in a material such as PMMA is of the order of microns. If adaptive re-meshing is not used as the crack propagates at high speed through the material, a uniform fine grid must

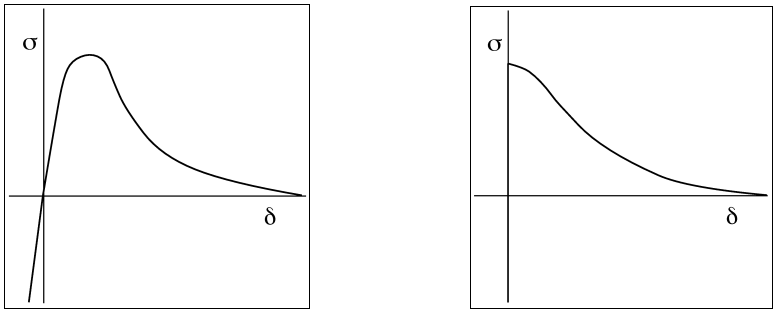

(a) (b)

Fig 1. (a). An initially elastic cohesive law. (b). An initially rigid cohesive law.

be employed across the entire width of the model and must extend to a sufficient height above and below the initial fracture plane to capture the evolving process region. On the other hand, the cohesive contribution to the stiffness should be small compared to that of the continuum cells. This can be difficult to achieve in practice when thousands of cohesive cells are inserted between the continuum cells in the fine grid region.

It has been shown in a recent work by the present authors [6] that the effect of this reduction in elastic stiffness can be so great as to completely rule out the use of this type of cohesive characteristic when studying the two dimensional evolution of the fracture process region. Two simulations were undertaken which clearly illustrate the effect of inserting cohesive cells of the type used by Xu and Needleman [5] between 13 micron square cells in a finite volume formulation. When a *single layer* of cohesive cells was used along the initial crack path, the predicted fracture load agreed with the experimental value and the crack accelerated quickly to a speed approaching the Rayleigh wave speed, as predicted by continuum fracture mechanics for a constant specific fracture energy. On the other hand, when many such layers were inserted in the fine grid region, both static and dynamic results were dramatically altered. The predicted fracture stress was reduced by about 40%, and the mean terminal crack propagation speed was reduced to about half the previous value. It was then demonstrated quite clearly for a wide range of cohesive parameters that the speed of crack propagation was of the order of the Rayleigh wave speed calculated on the basis of the modified Young's modulus of the material into which the cohesive cells had been inserted.

The alternative approach is to use a cohesive traction-separation law which has a descending part only, as was used in this context by Camacho and Ortiz [8]. Because there is no ascending part, the behaviour of the cohesive surface is initially rigid, as shown in Fig. 1(b). In practice, the cohesive cells are not inserted between the continuum cells at the beginning of the analysis as in the previous case. Instead, they are inserted only along the edges of elements whose traction reaches some critical value, which is usually defined as some combination of normal and shear stresses prevailing at that point in the continuum model. Because they are adaptively inserted as they are required, the elastic properties of the model are not altered in the same way as the first class of cohesive models described above and their use is therefore more appealing for process region modelling. The main disadvantages, of course, lie in the additional housekeeping that must be performed during the analysis. The tractions along the appropriate element edges need to be constantly monitored and checked against the failure criterion. In addition, the status and connectivity of the inserted cohesive cells must also be stored and updated for the duration of the analysis. This type of cohesive characteristic forms the basis of the current investigation.

A recent study by Falk et al. [7] addressed the issue of crack branching predictions in finite element models containing either cohesive cells with an initially elastic or an initially rigid traction-separation law. In both cases fully reversible cohesive behaviour was assumed. An important difference was noted between the crack propagation behaviour in the two models. In the models containing the initially rigid cohesive cells, the crack accelerated to a velocity which was very close to the Rayleigh wave speed, cohesive cells opened in a diffuse region around the crack tip, but no macroscopic branching was observed. On the other hand, in the models containing the initially elastic cohesive cells, the crack accelerated to a lower speed of about 75% of the previous value (presumably due to the reduction in stiffness

discussed above), then following a small reduction in speed, macroscopic branching into two separate cracks occurred. It was noted that since the separation criterion and its numerical implementation are key when the cohesive response is initially rigid, the possibility remained that the lack of branching in the former case was a consequence of the numerical implementation. It is important to note that a central-difference *explicit* time integration method was used in both cases. This differs from the current work, in which a *fully implicit* time integration scheme was employed.

2.3. On the importance of the shape of the traction-separation law

Recent research has shown that the *shape* of the cohesive law is of fundamental importance and can greatly influence the fracture behaviour of the material. This is not altogether surprising, as the shape of the curve ultimately reflects the physical separation processes occurring within the material. It does, however, represent a departure from the long-held view that the fracture process is characterised by Γ, the fracture resistance of the material, which is represented by the *area* under the traction-separation curve.

The influence of the shape of the cohesive law has been examined recently for quasi-static crack growth in elasto-plastic materials by Scheider and Brocks [9] and Li and Chandra [10], for quasi-static growth in brittle materials by Elices et al. [11], and for dynamic crack growth in brittle polymers by Bjerke and Lambros [12]. In the latter study, a single layer, thermally dissipative cohesive model was employed which was found to be in good agreement with experimental observation for low crack propagation rates. At higher crack speeds, however, a significant discrepancy was observed between predicted and measured values for each cohesive law considered. This suggests that at higher speeds the fracture process region is no longer small enough to be accurately modelled by a single layer cohesive zone model.

2.4. Determination of the cohesive parameters

In practice, the shape of the traction-separation law and the values of the cohesive parameters are determined in several ways. Where possible, the cohesive characteristics should be measured by means of appropriate tensile tests with the displacement being measured directly across the separating cohesive zone, as performed by Ting et al. [13] for polyethylene. There, a *family of curves* was obtained which more fully characterised the material cohesive behaviour for a range of different loading rates and degrees of constraint.

Indirect methods are also used, where the shape of the cohesive law is proposed in advance and a set of experiments is performed to determine the values of the relevant parameters, as described, for example, by Elices et al. [11]. Alternatively, use may be made of evolutionary search techniques to quantify the parameters in proposed cohesive laws to best reproduce experimental results, as described by Tin-Loi and Que [14].

Finally, the cohesive behaviour may be predicted from micromechanical models where available. One such study has been performed recently by Rottler et al. [15] which very effectively uses a combination of molecular dynamics and simple continuum fracture mechanics to calculate the macroscopic fracture energy of amorphous glassy polymers, such as PMMA.

3. Experimental test results

Two sets of experiments have been undertaken to study the dynamic fracture characteristics of cast sheets of PMMA using small single edge notched tensile (SENT) specimens. The first set [16,6,17] used a standard grade of material, whilst the second, more recent set examined the effect of molecular weight (M_w) on the dynamic fracture behaviour [18], as discussed below.

3.1. Fracture of standard molecular weight specimens

In the first set of tests, SENT specimens, 20 mm wide and 8 mm thick, were mounted in a universal testing machine with a grip spacing (gauge length) of 40 mm and extended at a rate of 2 mm/min, until specimen failure occurred. The notch depths ranged from 0.1 to 2.0 mm. Crack speeds were measured using both an electrical resistance method and high speed photography. The results are summarized in Figs. 2 and 3.

As shown in Fig. 2, the terminal crack speed is strongly dependent on the initial notch depth, with peak values of up to 800 m/s observed for the shortest notches. Specimens containing the 2.0 mm notches exhibited much lower crack speeds, with mean values of the order of 350 m/s. As has been reported elsewhere [19,20], the high-frequency crack speed oscillations have been found to correlate well with the fracture surface roughness, although as discussed in [6,17], a certain amount of filtering is usually required to remove noise from the crack speed signal, and this can have a significant influence on the results. In this case, a 'time-window' of 0.1 μs was chosen to resolve the highest-frequency physical crack speed oscillations that occurred during the fracture event. Fig. 3(a) shows the corresponding fracture surfaces for the results presented in Fig. 2. The specimen containing the 2.0 mm notch exhibited a smooth mirror-like surface, while at shorter notch depths the visible damage increased until, at a notch depth of 0.1 mm, the entire surface had a flake-like structure indicative of micro-cracking beneath the surface. The structure of the fracture surface in this region is revealed by the scanning electron micrographs shown in Figs. 3(b) and (c).

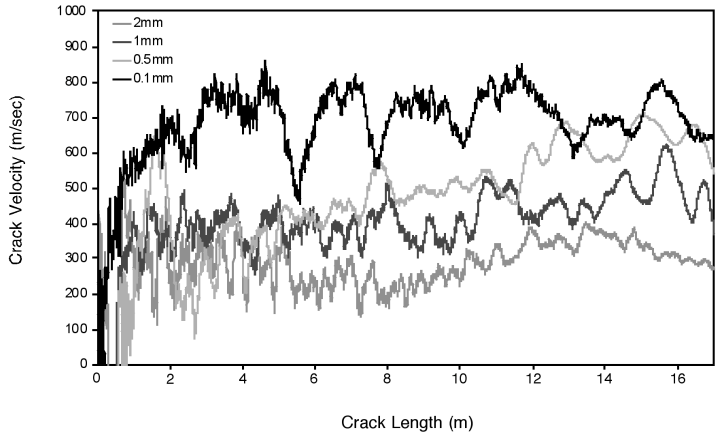

Fig. 2. Crack speed data for 40 × 20 × 8 mm SENT specimens of standard molecular weight PMMA [16].

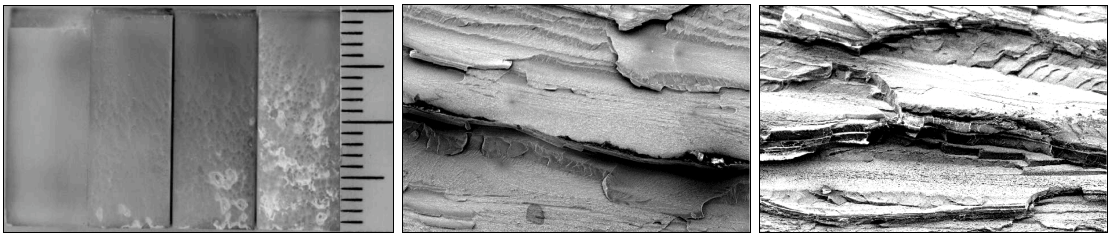

(a) (b) (c)

Fig. 3. (a). Corresponding fracture surfaces for standard M_w specimens [16]. In each case the crack has propagated from top to bottom. Notch sizes are 2.0 mm (left specimen), 1.0 mm, 0.5 mm, and 0.1 mm (right specimen). The scale shown on the right is in mm. (b). Scanning electron micrographs of typical fracture surfaces in the flaky region [22]. Magnification $\times 110$, field of view 1.2×0.8 mm. (c). Magnification $\times 170$, field of view 0.75×0.5 mm.

3.2. The effect of varying molecular weight

A second set of experiments was carried out to assess the effect of varying the molecular weight on the dynamic fracture characteristics. Three grades of PMMA were considered: low (1.4×10^5 g/mol), standard ($1\text{-}2 \times 10^6$ g/mol), and high (5×10^6 g/mol) molecular weight. In these tests, specimen dimensions of $20 \times 20 \times 3$ mm were used. In addition, notch depths of 0.1 mm, 0.5 mm and 1.0 mm were considered. Although these specimen dimensions are different to both the previous set of tests and the numerical simulations that follow, it is of interest to note the main conclusions of this study for future reference.

Firstly, it was found that the fracture stress was essentially independent of M_w. Furthermore, the crack speed characteristics for the high and standard M_w specimens were similar to the values shown in Fig. 2. However, the crack speeds recorded for the low M_w specimens were considerably higher than those for the other grades. Those associated with the 1.0 mm notches averaged 650 m/s, whilst values close to the Rayleigh wave speed were observed for the 0.1 mm notch depths. In addition, it was found that the surface roughness increased dramatically as the molecular weight decreased, as shown in Fig. 4. This is possibly related to the amount of free volume present at a molecular level in this grade of material, as proposed by Newman and Wolock [21]. Shorter chain lengths are associated with an increased number of chain ends which may act as nucleation sites for micro-cracks. Finally, crack bifurcation was observed in the low M_w specimens containing the 0.1, the 0.5 mm and occasionally the 1.0 mm notches.

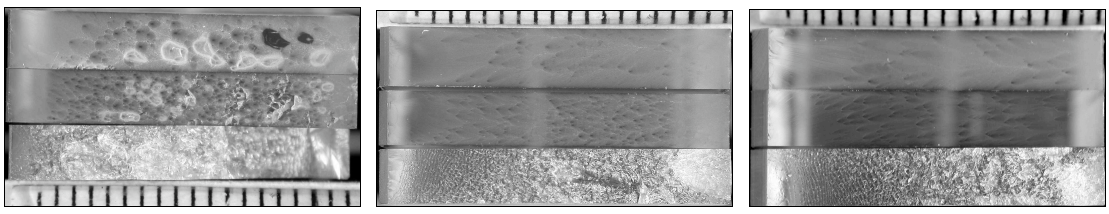

(a) (b) (c)

Fig. 4. Fracture surface appearance of (top to bottom in each case) high, standard and low molecular weight specimens. (a). 0.1 mm notch. (b). 0.5 mm notch. (c). 1.0 mm notch [18].

Table 1
Observed failure strength of notched SENT specimens [16,18]

Notch Depth (mm)	Mean Fracture Stress (MPa)	Standard Deviation (MPa)
0.1	43.8	3.3
0.5	26.0	2.2
1.0	20.8	2.9
2.0	12.5	1.1

3.3. Combined static results for both series of tests

As mentioned above, it was found that the fracture stress was virtually independent of the molecular weight of the specimens in this range. Eleven valid tests were carried out for each set of specimens containing the 0.1, 0.5 and 1.0 mm notches, whilst only two reliable results were obtained for those containing the 2.0 mm notches. Many more tests were carried out but the results were discarded as an unacceptable level of specimen or grip misalignment was observed. The experimental observations are summarized in Table 1.

4. Numerical investigations

A finite volume formulation was used to simulate the dynamic fracture of the PMMA specimens [23,24,6,25]. The evolution of the fracture process region was modelled for the first 10 mm of crack growth using four different cohesive characteristics. Even though the fracture energy and the cohesive strength were held fixed in each case, the dynamic fracture behaviour was found to be strongly dependent on the shape of the cohesive law.

4.1. Model geometry

To reduce the computational effort, a 10×40 mm SENT model was considered, as shown in Fig. 5. This model is intended to represent one half of the 20×40 mm experimental specimens in [16]. Symmetry boundary conditions were applied to the right hand edge of the model, the bottom edge was held fixed, whilst the displacement (static analyses) or the velocity (transient analyses) were specified along the top edge. The left hand edge containing the initial notch was assumed to be traction-free. A uniform fine grid region was defined, which spanned the width of the model and whose height extended an equal distance above and below the initial fracture plane. The appropriate height of the fine grid region depended on the notch depth and the cohesive characteristic employed, and had to be large enough to contain the evolving fracture process zone. The height of this region ranged from 3 to 6 mm. Within the fine grid region, a square cell size of 10×10 μm was used. Outside this region, the height of the cells increased gradually to 0.8 mm at the top and bottom of the model. The number of continuum cells in the models ranged from 388,000 to 688,000, depending on the size of the fine grid region. Plane strain conditions were assumed.

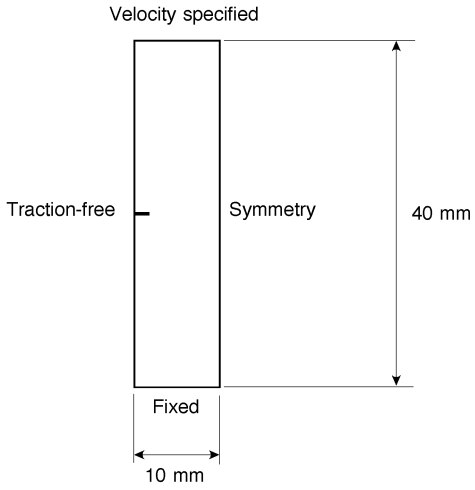

Fig. 5. Dimensions of model considered and associated boundary conditions.

4.2. Analysis procedure

The analysis procedure may be summarized as follows. At the end of a given time step, the tractions across the faces of each continuum cell were evaluated and if the failure criterion was satisfied anywhere in the model, cohesive cells were inserted between the continuum cells adjacent to this face. The time step was then repeated so that a converged solution was obtained for the model containing the recently-added cohesive cells before proceeding to the next time step. In this investigation, a purely tensile failure criterion was assumed. Hence the cohesive cells were inserted if the normal traction was greater than or equal to the cohesive strength.

4.3. Cohesive characteristics

Four different, rate-independent, cohesive characteristics were considered, as shown in Fig. 6(a)-(d). The cohesive strength and separation energy were held constant at 80 MPa and 355 J/m^2 respectively. These represent typical mean values quoted in the literature [26,27]. It is worth noting in particular that Kusy and Turner [26] observed a sharp decrease in the fracture energy of PMMA when the molecular weight was reduced below 1×10^5 g/mol. Above this level, the fracture energy was found to be essentially independent of M_w.

The main parameter under investigation in this study was the slope of the initial portion of the softening curve. For each of the three descending traction-separation laws, the initial slope became progressively steeper by a factor of two in each case, whilst the critical separation was held constant at 8.8 μm. In addition, it is worth emphasising that the cohesive constitutive relations were taken to be initially rigid in each case, and that the elastic properties of the model were therefore unaffected prior to the insertion of the cohesive cells.

The cohesive behaviour may be summarized as follows. When the normal opening displacement δ increases monotonically, the normal cohesive traction σ decreases according to the cohesive laws in Fig. 6 (a)-(d). If, after some opening displacement δ^*, unloading takes place, then the tractions obey the linear unloading relation shown in Fig. 6(b). If subsequent reloading takes place, the unloading path is reversed until

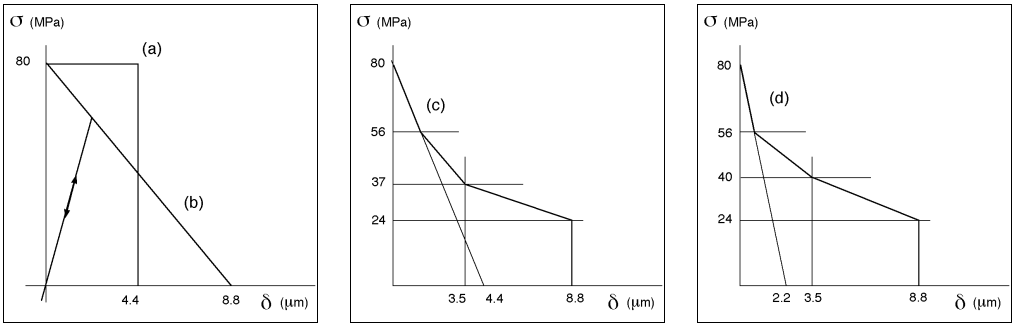

Fig. 6. Assumed cohesive characteristics. (a). Constant stress. (b). Linearly descending (including unloading behaviour). (c). Trilinear. (d). Steeper trilinear.

the displacement δ^* is reached, and subsequently the monotonic cohesive relations are followed again. When the critical normal separation is reached, fracture is assumed to have taken place and the cell faces are thereafter treated as traction-free surfaces.

The shear traction across the cohesive surfaces is computed as follows. Before the cohesive cells are inserted between the faces of the adjacent continuum cells, the prevailing shear traction on this plane is noted. Let this value be τ_o. After the cohesive cells have been inserted, the shear traction corresponding to a given normal traction σ is simply taken to be

$$\tau = \frac{\sigma}{\sigma_{coh}} \tau_o , \tag{1}$$

where σ_{coh} is the cohesive strength of the material. Hence, the shear characteristic has the same shape as the normal characteristic. This is essentially the same cohesive behaviour as assumed by Camacho and Ortiz [8].

4.4. Static Results

The laboratory tests were performed under static loading conditions, and so the behaviour of the model both prior and subsequent to the onset of unstable crack growth is of interest. The former phase was simulated using a static analysis, whilst the latter, rapid crack propagation, phase required a transient analysis to be performed. Whilst a transient analysis could have been used from the outset, the very low rate of extension would have resulted in an unnecessarily long run time prior to fracture initiation. Results of interest from the static analysis include the applied stress at the onset of unstable crack growth, the associated J-integral [28] and strain energy values, and the length of the craze region ahead of the stationary crack tip under these loading conditions.

In the static phase of the analysis, the model was loaded by applying displacement increments to the top face. When the traction across the cell face directly ahead of the crack tip reached the cohesive strength, a cohesive cell was inserted between the adjacent continuum cells, as described above. This procedure continued until the point where unstable crack growth was imminent, when the magnitude of the applied incremental displacements was considerably reduced to allow the final stages of craze formation to be accurately modelled. Eventually, the analysis failed to converge and

the static results were recorded. The J-integral was computed around several contours and path independence was noted in every case.

The craze length was defined as the number of cohesive cells which had been inserted ahead of the crack tip at the last converged solution step. As the length of the cell faces in the fine grid region was 10 μm, the resolution of the craze length was obviously restricted to this value. Finally, the mean axial stress at the grips was computed for comparison with the experimental data. The static results for each of the four cohesive laws considered are summarized in Tables 2 to 5.

4.4.1. Discussion

In most cases, the experimental and numerical results are in close agreement. The only case where the predicted fracture stress was well outside the observed range of experimental values occurred for the 0.1 mm notch using the constant stress cohesive law. In general, the three descending cohesive laws (Tables 3-5) predicted fracture

Table 2
Static results for constant stress cohesive law

Notch Depth (mm)	Fracture Stress (MPa)	J-Integral (J/m^2)	Strain Energy (J/m thickness)	Craze Length (μm)
0.1	51.1	349	138	100
0.5	25.4	354	35	90
1.0	18.5	355	18	80
2.0	13.0	349	9	80

Table 3
Static results for linearly descending cohesive law

Notch Depth (mm)	Fracture Stress (MPa)	J-Integral (J/m^2)	Strain Energy (J/m thickness)	Craze Length (μm)
0.1	45.4	328	107	140
0.5	24.6	354	32	150
1.0	18.1	355	17	150
2.0	13.0	355	9	150

Table 4
Static results for trilinear cohesive law

Notch Depth (mm)	Fracture Stress (MPa)	J-Integral (J/m^2)	Strain Energy (J/m thickness)	Craze Length (μm)
0.1	40.2	318	87	190
0.5	23.9	354	31	200
1.0	17.8	355	17	190
2.0	12.9	355	9	190

Table 5
Static results for steeper trilinear cohesive law

Notch Depth (mm)	Fracture Stress (MPa)	J-Integral (J/m^2)	Strain Energy (J/m thickness)	Craze Length (μm)
0.1	40.0	314	86	210
0.5	23.9	354	31	210
1.0	17.7	354	17	200
2.0	12.9	355	9	200

strengths which were lower than the mean experimental value. Closer agreement would have been achieved if a higher cohesive strength had been chosen for these cases, perhaps increasing this parameter to 90 MPa. Of particular interest is the variation of elastic strain energy as a function of notch depth. The energy stored in a specimen containing a 0.1 mm notch is an order of magnitude greater than that associated with a 2.0 mm notch. It will be shown that a relatively high value of stored energy is a necessary condition for branching to take place during subsequent rapid crack propagation.

For the three descending cohesive laws (Tables 3-5), it was found that the value of the path-independent J-integral was approximately equal to the separation energy at the onset of crack growth for notch depths of 0.5 mm and above, regardless of the shape of the cohesive law. For the shortest notches, the length of the cohesive zone is no longer small in comparison to the notch depth and the equivalence of the Griffith and cohesive theories of fracture no longer holds [28]. It would be expected, of course, that the value of the J-integral would be exactly equal to the fracture energy at the onset of unstable crack growth. It is worth emphasising that the static analyses were terminated when convergence failure occurred and these results therefore represent the point of numerical instability rather than that of fracture initiation.

The results for the constant stress (or Dugdale [29]) cohesive law deserve closer inspection. If the length of the cohesive zone is small compared to the crack length, it may be shown that the length of this region is given by

$$R_p = \frac{\pi}{8}\frac{K_{\mathrm{I}}^2}{\sigma_{coh}^2}, \tag{2}$$

where σ_{coh} is the (constant) cohesive stress. This equation may be used to check the magnitude of the craze length for the deeper notches. The stress intensity factor for an SENT specimen containing a small edge crack is given by [27]

$$K_{\mathrm{I}} = 1.12\sigma\sqrt{\pi a}, \tag{3}$$

where σ is the applied stress and a is the crack length. For a cohesive strength of 80 MPa, the lengths of the cohesive zones associated with the 1.0 mm and 2.0 mm notches are predicted to be 82.7 μm and 81.7 μm, respectively. These values compare very well to the numerical predictions of 80 μm in each case, given that the cohesive cell size was 10 μm in the numerical models.

Two further points may be made regarding the computed craze lengths. Firstly, it should be noted that the length of the static cohesive zone increases quite substantially for the decreasing traction-separation laws, reaching 200 μm in the case of the steeper trilinear curve. Secondly, Tables 2 to 5 show that craze lengths for the 1.0 and 2.0 mm notches are equal to each other for all four of the cohesive characteristics. This corresponds to a condition of autonomy near the crack tip, where the same development of processes at the tip are observed for different specimen and loading geometries. As pointed out by Broberg [2], all the different concepts used in linear elastic fracture mechanics (LEFM) are developed explicitly or tacitly under the assumption of autonomy, which thus provides the very basis for LEFM.

4.5. Dynamic results

The subsequent rapid crack propagation phase was then simulated for each cohesive characteristic in turn, and the results are presented below. In each case the top face of the model was subjected to the experimental loading rate of 3.3×10^{-5} m/s (or 2 mm/min). Results of particular interest from the transient analysis include the variation of crack front velocity, crack paths, branching and the accumulated damage as a function of crack length.

The results will be presented in the following manner. Firstly, a fixed specimen geometry will be considered whilst the cohesive law is varied. The most appropriate traction-separation law will then be determined by comparison with experimental results. This cohesive characteristic will then be used to examine the influence of notch depth on the dynamic fracture characteristics of the models.

4.5.1. Notch depth 0.1 mm with varying cohesive characteristics

The damage evolution in the fine grid region of each model is shown in Fig. 7. The corresponding crack speed histories are shown in Fig. 8. As noted above, a certain amount of processing was performed on the experimental crack speed data. For ease of comparison, the simulated crack speed histories were also smoothed using a 0.1 μs time-window.

For each cohesive law, the crack growth is characterised by a period of initial acceleration up to a mean terminal velocity below the Rayleigh wave speed. During this initial period, the crack is confined to its initial plane and the fracture surface in this region is perfectly flat with no subsurface damage. Thereafter, the extent of the subsurface damage increases and the crack speed exhibits characteristic high frequency oscillations.

It is clear from Figs. 7(a) and 8(a), however, that the predictions obtained using the Dugdale-type cohesive law are unrealistic for this material. After an initial acceleration to about 540 m/s, the crack quickly decelerates to 240 m/s after 1.7 mm of growth. At this stage the single planar crack is replaced by two parallel cracks and the crack speed curve becomes difficult to interpret. The simulation was subsequently stopped after 5.6 mm of crack growth. The predictions obtained from the descending cohesive characteristics, however, are much more realistic and compare well with the experimentally recorded crack speed data in Fig. 2 for this notch depth.

It is also of interest to compare the crack branching predictions obtained in each case. In the linearly descending case (Fig. 7(b)), successive attempted branching events are observed after 1 mm and 2 mm of crack growth, and macroscopic branching is achieved after about 3.5 mm of growth. The results for the two trilinear characteristics are quite similar to each other, as shown in Figs. 7(c) and (d). Attempted branching takes place after 5-6 mm of crack growth, and again after 7.5 mm. However, as the slope of the cohesive characteristic becomes steeper, the terminal crack speed increases and the extent of the damage decreases.

Crack bifurcation was experimentally observed in the low molecular weight material for the specimens containing 0.1mm and 0.5 mm notches. Indeed, the onset of bifurcation occurred after approximately 3 mm of crack growth for the former specimens, as shown in Fig. 9. This compares very well to the numerical predictions for the linear descending cohesive law, as shown in Fig. 7(b). Furthermore, the extent of the crack deviation from the mid-plane predicted by both the linear descending and

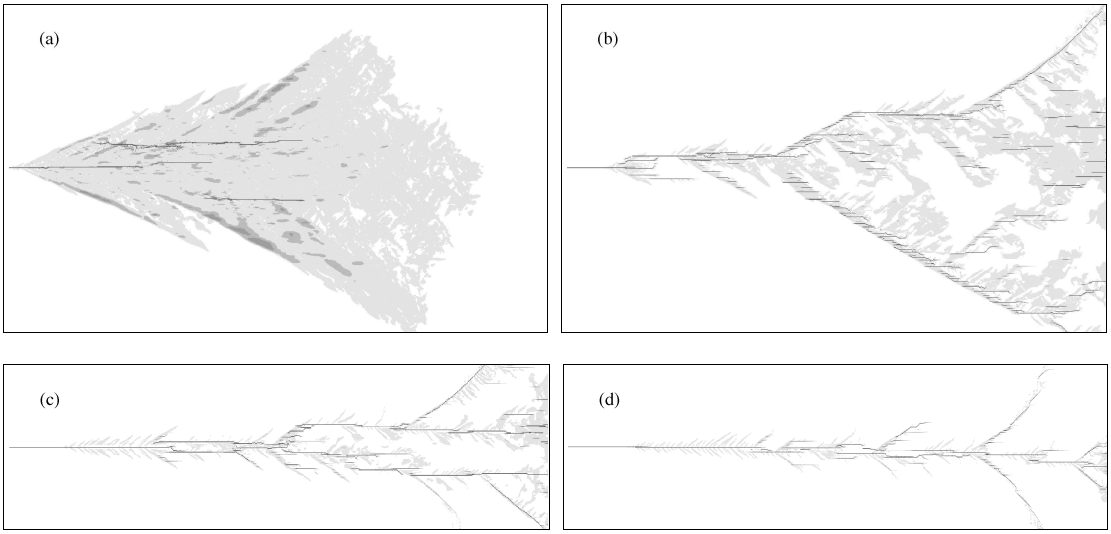

Fig. 7. Crack path and damage evolution for 0.1 mm notches using various cohesive laws. (a). Constant stress – simulation stopped at 5.6 mm. (b). Linearly descending. (c). Trilinear. (d). Steeper trilinear. Window sizes 10 mm × 6 mm for (a) and (b), and 10 mm × 3 mm for (c) and (d). Legend: Light grey – cohesive separation 0 to 20% of fully-separated value, Mid-grey: 20 to 40%, Dark grey: 40 to 99%, Black: fully broken.

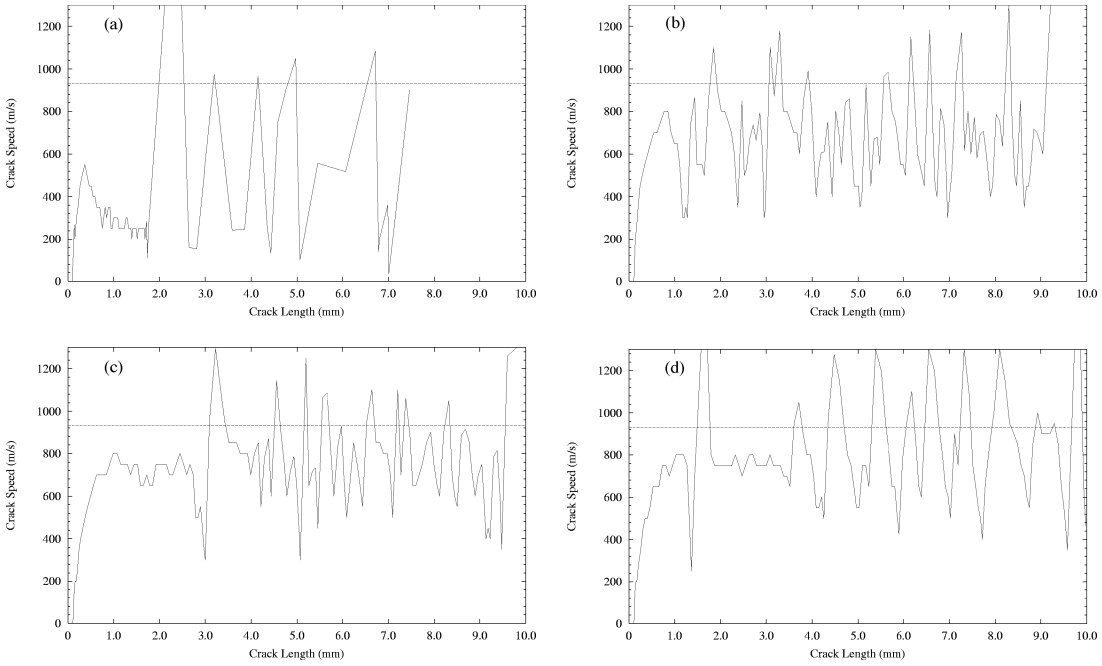

Fig. 8. Corresponding crack speed histories for 0.1 mm notches. (a). Constant stress. (b). Linearly descending. (c). Trilinear. (d). Steeper trilinear. The Rayleigh wave speed of 930 m/s is also shown.

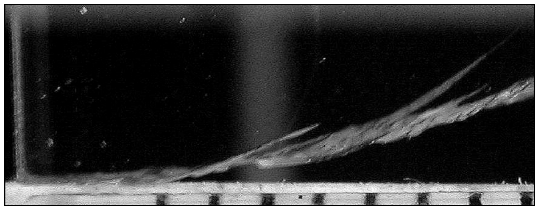

Fig. 9. Crack bifurcation in a 20 mm wide, low molecular weight specimen containing a 0.1 mm notch [18]. For ease of comparison with the numerical results, only the first 10 mm of crack growth is shown, after which the crack has deviated approximately 2 mm from the mid-plane.

the trilinear characteristics are very close to the experimental observation of 2-3 mm after 10 mm of crack growth. Finally, it is worth noting with reference to Fig. 9, that the majority of the damage is confined in practice to a relatively narrow region on either side of the fracture surface. In this regard, the extensive damage predicted in Figs. 7(a) and (b) may be regarded as less realistic than that produced by the steeper cohesive characteristics in Figs. 7(c) and (d). For this reason, the trilinear cohesive law, as shown in Fig. 6(c), will be employed to examine the influence of notch depth on the dynamic fracture characteristics of the models.

4.5.2. Trilinear cohesive characteristic with varying notch depths

In this case, the damage evolution in the fine grid region of each model is shown in Fig. 10, and the corresponding crack speed histories are shown in Fig. 11. Clearly, as the notch depth decreases, the extent of the surface roughness and subsurface damage increases substantially, with attempted and successful branching predictions for the shorter notches. This corresponds well to the experimentally observed fracture surfaces in Figs. 3 and 4. The markedly different behaviour of the models containing the 0.1 mm and the 2.0 mm notches is not surprising, given the associated strain energy levels in each case, as shown in Table 4. As a result, the energy flow to the crack tip region increases substantially as the notch size decreases with a corresponding increase in the size of the fracture process region.

Referring to Fig. 11, it may be seen that both the initial rate of acceleration of the crack tip and the mean terminal velocity are predicted to increase significantly as

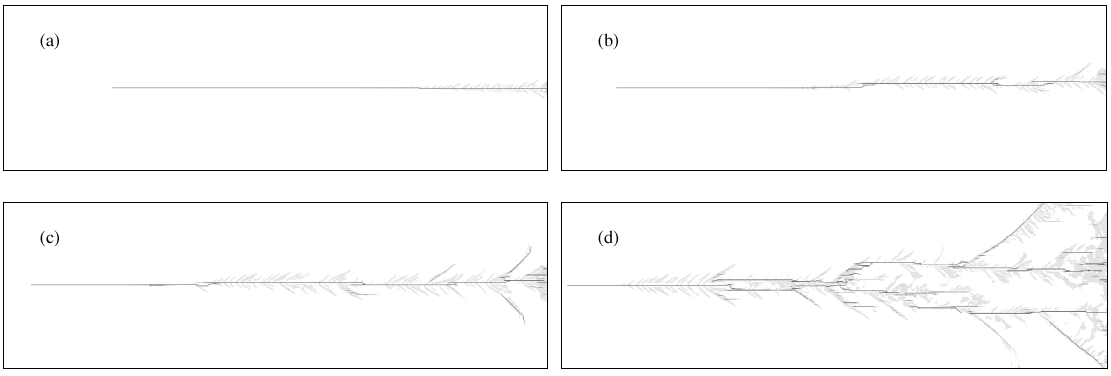

Fig. 10. Crack path and damage evolution for various notch depths using the trilinear cohesive law. (a). 2.0 mm notch. (b). 1.0 mm notch. (c). 0.5 mm notch. (d). 0.1 mm notch. Window size 10 mm × 3 mm. Legend as in Fig. 7.

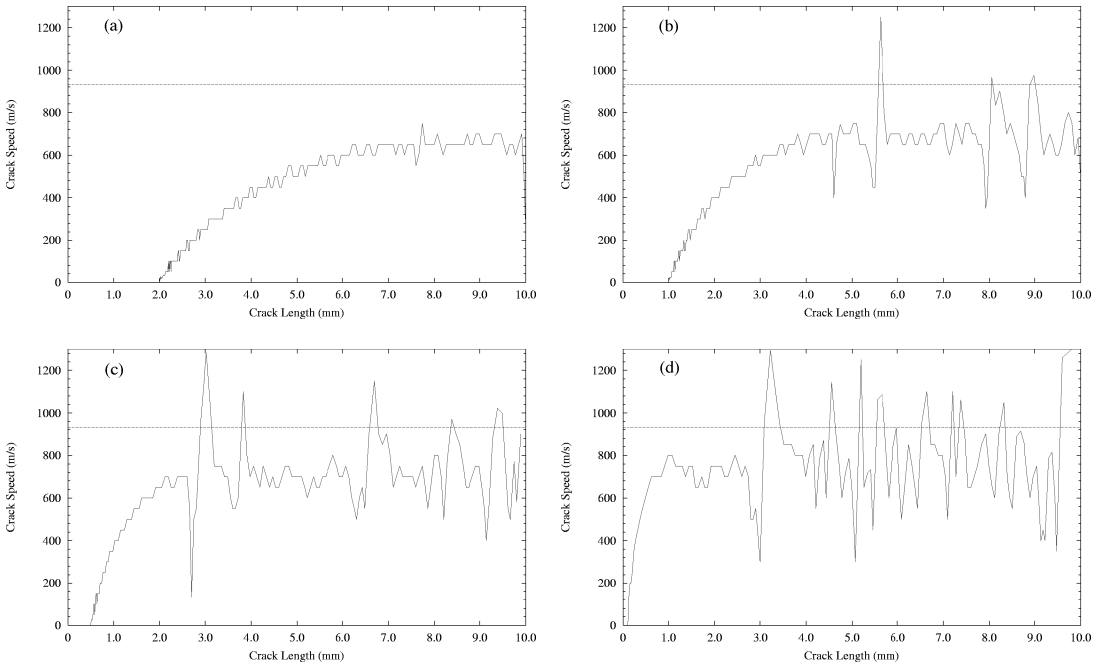

Fig. 11. Corresponding crack speed histories for various notch depths using the trilinear cohesive law. (a). 2.0 mm notch. (b). 1.0 mm notch. (c). 0.5 mm notch. (d). 0.1 mm notch. The Rayleigh wave speed of 930 m/s is also shown.

the notch depth decreases. Here again, the initial featureless phase of crack propagation is associated with a relatively smooth velocity history, with the onset of subsurface damage being accompanied by high frequency velocity oscillations.

4.5.3. Discussion

It is of interest to compare the experimental results with the numerical predictions for each notch depth. In the case of the standard and high M_w specimens, the mean crack speeds varied from 350 m/s to 800 m/s as the notch depth was decreased from 2.0 to 0.1 mm respectively. The observed speeds for the low M_w specimens ranged from 650 m/s for the 1.0 mm notches to over 900 m/s for the 0.1 mm notches prior to bifurcation. Clearly, the predicted crack speed histories for the descending cohesive laws most closely match the behaviour of the *low* M_w material.

In general, however, it is clear that an improved cohesive description of these materials is required. The underlying physics of the fracture process region are complex and undoubtedly depend on such factors as the rate of separation, the degree of constraint, the local temperature and the molecular weight of the material. The development and calibration of such models must be the subject of future research if further progress is to be made in this area.

5. Conclusions

This cohesive formulation has enabled many experimental observations to be both qualitatively and quantitatively reproduced. These include the prediction of fracture stress under static loading conditions, the acceleration of the crack tip from rest to velocities well below the Rayleigh wave speed, and the subsequent dynamic crack

propagation at constant mean terminal velocities under conditions of increasing energy flux to an expanding process region. In addition, characteristic high frequency velocity fluctuations associated with the initiation of subsurface damage were obtained, along with attempted and successful branching events. The variation of all of these quantities was examined as a function of notch depth and the correct trends were predicted.

In particular, the simulations involving the descending cohesive laws most closely matched the behaviour of the *low* M_w specimens, where higher crack speeds and crack bifurcation were observed for the shorter notches. The Dugdale-type cohesive law was found to be unsuitable in this context, the dynamic fracture behaviour being characterised by excessively low crack speeds and extensive subsurface damage.

The results clearly show that the dynamic fracture simulations are sensitive to the shape of the cohesive law. This is clearly emphasised for shorter notches, where the energy in the system is an order of magnitude higher than that associated with the deeper notches. In particular, it has been found that the initial slope of the decreasing part of the cohesive law is an important parameter, and quite different behaviour was observed for the three descending cohesive laws, in spite of the fact that the cohesive strength, fracture energy and critical separation values were constant in each case. As the slope became steeper, the terminal crack speed increased and the extent of the damage decreased.

References

[1] Freund LB. Dynamic fracture mechanics. Cambridge University Press; 1990.

[2] Broberg KB. Cracks and fracture. San Diego, CA: Academic Press; 1999.

[3] Ravi-Chandar K. Dynamic fracture of nominally brittle materials. Int J Fract 1998;90:83-102.

[4] Klein PA, Foulk JW, Chen EP, Wimmer SA, Gao HJ. Physics-based modeling of brittle fracture: cohesive formulations and the application of meshfree methods. Theoret Appl Fract Mech 2001;37:99-166.

[5] Xu XP, Needleman A. Numerical simulations of fast crack growth in brittle solids. J Mech Phys solids 1994;42:1397-1434.

[6] Ivankovic A, Murphy N, Hillmansen S. Evolution of dynamic fractures in PMMA: experimental and numerical investigations. In: Aliabadi MH, Ivankovic A, editors. Crack dynamics. Advances in fracture mechanics, vol. 9. Southampton, UK: WIT Press/Computational Mechanics Publications; 2004.

[7] Falk ML, Needleman A, Rice JR. A critical evaluation of cohesive zone models of dynamic fracture. J Phys IV, France 2001;11:Pr5-43-50.

[8] Camacho GT, Ortiz M. Computational modeling of impact damage in brittle materials. Int J Solids Struct 1996;33:2899-2938.

[9] Scheider I, Brocks W. The effect of the traction separation law on the results of cohesive zone crack propagation analyses. Key Engineering Materials 2003;251-252:313-318.

[10] Li H, Chandra N. Analysis of crack growth and crack tip plasticity in ductile materials using cohesive zone models. Int J Plast 2003;19:849-882.

[11] Elices M, Guinea GV, Gomez J, Planas J. The cohesive zone model: advantages, limitations and challenges. Eng Fract Mech 2002;69:137-163.

[12] Bjerke TW, Lambros J. Theoretical development and experimental validation of a thermally dissipative cohesive zone model for dynamic fracture of amorphous polymers. J Mech Phys Solids. 2003;51:1147-1170.

[13] Ting SKM, Williams JG, Ivankovic A. Effects of constraint on the traction-separation behaviour of polyethylene. In: Blackman BRK, Pavan A, Williams JG, editors. Fracture of polymers, composites and adhesives II. ESIS publication 32. Elsevier; 2003;143-154.

[14] Tin-Loi F, Que NS. Identification of cohesive crack fracture parameters by evolutionary search. Comput Meth Appl Mech Eng 2002;191:5741-5760.

[15] Rottler J, Barsky S, Robbins MO. Cracks and crazes: on calculating the macroscopic fracture energy of glassy polymers from molecular simulations. 2002; e-print cond-mat/0112006.
[16] Manmek S. Experimental investigation of crack tip velocity variations. MSc Thesis. Imperial College, London. 1999.
[17] Ivankovic A, Hillmansen S. Evolution of dynamic fractures in poly(methyl methacrylate). Plast Rubber Compos 2001;30:88-93.
[18] Al-Hamdani B. Investigating the damage and fracture characteristics of PMMA specimens of varying molecular weights. MSc Thesis. Imperial College, London. 2003.
[19] Fineberg J, Gross SP, Marder M, Swinney HL. Instability in dynamic fracture. Phys Rev Lett 1991;67:457-460.
[20] Fineberg J, Gross SP, Marder M, Swinney HL. Instability in propagation of fast cracks. Phys Rev B 1992;45:5146-5153.
[21] Newman SB, Wolock I. Fracture phenomena and molecular weight in polymethyl methacrylate. J App Phys 1958; 29:49-52.
[22] Scanning electron micrographs produced at the Institute of Materials Research Engineering, Singapore.
[23] Demirdzic I, Muzaferija S. Finite volume method for stress analysis in complex domains. Int J Num Meth Eng 1994;37:3751-3766.
[24] Ivankovic A. Finite volume modelling of dynamic fracture problems. Comput Model Simulat Engng 1999; 4:227-235.
[25] Ivankovic A, Pandya KC, Williams JG. Crack growth predictions in polyethylene using measured traction-separation curves. Eng Fract Mech 2004;71:657-668.
[26] Kusy RP, Turner DT. Influence of the molecular weight of poly(methyl methacrylate) on fracture surface energy in notched tension. Polymer 1976;17:161-166.
[27] Williams JG. Fracture mechanics of polymers. Ellis Horwood;1984.
[28] Rice JR. A path independent integral and the approximate analysis of strain concentration by notches and cracks. J Appl Mech 1968;35:379-386.
[29] Dugdale DS. Yielding of steel sheets containing slits. J Mech Phys Solids 1960;8:100-104.